Non-destructive I*n-Operando* Investigation of Catalyst Layer Degradation for Water Electrolyzers using Synchrotron Radiography

Olha Panchenko[a], Marcelo Carmo[a,*], Marcin Rasinski[b], Tobias Arlt[d], Ingo Manke[c], Martin Müller[a], Werner Lehnert[a,e]

Forschungszentrum Jülich GmbH, Institute of Energy and Climate Research – Electrochemical Process Engineering (IEK-3), 52425 Jülich, Germany
Forschungszentrum Jülich GmbH, Institute of Energy and Climate Research – Plasma Physics (IEK-4), 52425 Jülich, Germany
[c] Helmholtz-Zentrum Berlin GmbH, Institute of Applied Materials, Berlin, Germany
[d] Technische Universität Berlin, Berlin, Germany
[e] Faculty of Mechanical Engineering, RWTH Aachen University, Aachen, Germany

* m.carmo@fz-juelich.de

Abstract

Unveiling degradation mechanisms is a difficult task encountered when characterizing materials and components for water electrolyzers, where for stationary applications these cells are expected to run for 50.000 hours or more. From a R&D perspective, this incredibly long time-dependence makes the assessment of degradation mechanisms almost impracticable. Therefore, novel and advanced methodologies need to be demonstrated, aiding scientists to more quickly identify and effectively tackle the different stressors that lead to degradation. Here we show a novel approach where *in-operando* synchrotron radiography was used to access real-time electrode degradation. A real catalyst-coated membrane was assembled and tested under real water splitting conditions, where iridium catalyst detachment could be observed and semi-empirically quantified. For the first-time, we have also demonstrated a way to visualize and identify where bubble formation inside the catalyst-coated membrane occurs, and how it can trigger electrode degradation. This study shall open new avenues to quickly and properly unveil degradation mechanisms, methods that could also be used for other electrochemical devices such as batteries, fuel cells and solar water splitting technologies.

1. Introduction

Our future energy supply is inevitably going to be dependent on renewable energy sources such as wind turbines and photovoltaics [1, 2]. However, these power sources are obviously weather-dependent, and therefore energy storage solutions under the same magnitude are required [3]. Consequently, hydrogen production using polymer electrolyte membrane (PEM) water electrolyzers is foreseen as the only solution to store large amounts of electricity [4, 5]. However, when using electrochemical systems for stationary applications, the challenge to demonstrate cost-effective components for PEM electrolyzers [6] that can reliably run for 50.000 to 100.000

hours or more still remains [7-9]. We also recognize that the core component of a PEM water electrolyzer – the cathode coated membrane (CCM), rules over cell efficiency and durability. The CCM comprises of a proton-conducting membrane (typically Nafion from Chemours®) and two catalysts layers working as electrodes. Platinum and iridium are mainly used as catalysts [4, 10], and makes up a large proportion of the total cost of an electrolyzer, namely 24 % of all stack costs [11].

To date, the different degradation processes occurring in a CCM have only been extensively described for PEM fuel cells [12-14]. Laconti et al. [15] for instance distinguishes between the chemical and mechanical influences on membrane degradation. In their studies, the mechanical stress factors included thermal membrane expansion as well as damage to the membrane through the gas diffusion layer surface. Chemical stress is caused by the formation of peroxyl radicals, which attack the membrane backbone. Different publications have also reported that higher temperature also accelerates the chemical degradation processes. Different research groups have [13, 16-18] also described the degradation mechanism in which platinum diffuses through the membrane. This aging phenomenon is known as the "platinum-band formation" and has been consistently described in PEM fuel cell literature as well.

Similar degradation processes could occur during the operation of a PEM electrolysis cell. Debe at al. [19] detected platinum particles used as a cathode catalyst on the anode side after 1500 hours of operation. Iridium also diffused from the anode side to the cathode side, and showed a 40 % increase in crystallite size over time. Elemental analysis indicated that two conversion processes occurred: the anode catalyst iridium diffused to the cathode side and the cathode catalyst platinum diffused to the anode side, i.e. catalyst migration in the respective opposite directions. However, neither platinum nor iridium particles were detected inside the membrane. Agglomeration and particle growth on the cathode side (platinum on carbon black Pt/C) was also observed in some of our studies [20].

When specifically considering electrocatalysts degradation, aging and degradation processes are generally indicated by a reduction of electrochemically active surface area (ECSA) of a given catalyst nanoparticle. Platinum particles for instance can migrate over the carbon support and form agglomerates, with a consequent reduction of ECSA [14]. Due to additional degradation process, also known as Ostwald ripening [21], the particles grow to even larger agglomerates, further reducing ECSA or catalyst utilization. Nanoparticles can also detach from the carbon support and lose their electrical contact to the electrode, meaning that the catalyst particles are no longer available for the electrochemical reaction. In addition to loss of ECSA, catalyst poisoning can also be an issue, usually related to underpotential deposition of other metals on the nanoparticles [22] present in the water stream into the electrolyzer.

Mayrhofer et al. [23] developed a non-destructive method using transmission electron microscopy (TEM) to observe the changes in the catalyst structure before and after electrochemical tests. Catalysts were clearly affected by the electrochemical condition, and several degradation phenomena such as the detachment of particles, the movement of particles

within the layer, and agglomeration processes were observed. A complete detachment of the platinum catalyst from the substrate was also shown without subsequent re-deposition [24], which contradicts the aforementioned Ostwald ripening. This method was later used in our group to observe the mobility of platinum nanoparticles over the carbon support, this time under electrolysis behaviour [25].

Other degradation investigations are conducted using a typical rotating disc electrode (RDE) setup, where the catalyst particles are deposited on a glassy electrode or flat substrate and inserted in a liquid electrolyte [26]. Unfortunately, under real cell conditions, the catalyst layer is additionally subjected to other factors such as mechanical stress. A real electrolysis CCM electrode is also manufactured onto totally different structure conditions, where the catalyst is bound to a solid but humidified membrane, fixed by Nafion working as a binder, and subjected to mechanical stress by the porous transport layer (PTL). Under real conditions, the membrane expands considerably depending on cell operating conditions. During catalyst coating, cracks emerge and particles at the boundary suffer from mechanical stress and can detach or delaminate [27-29]. An additional contributory factor is the PTL surface that comes into direct contact with the catalyst layer. PTLs with high porosity levels often have a very rough surface, which can critically mechanically affect the catalyst layer. In addition, the issue of titanium passivation over-time can only be prevented by using noble metal coatings on the PTL [29]. The influence of current density on degradation is also relevant, where severe gas evolution can mechanically affect the integrity of the catalyst layer.

All these degradation mechanisms are generally triggered after long-term operation, and the complexity of a single-cell platform makes it even more difficult to access materials degradation. We therefore consider of high relevance the development of novel methods to precisely observe the degradation effects occurring to CCM architectures and its materials. Here we demonstrate a novel approach that allows a real-time investigation of the degradation effects of catalyst layers using synchrotron radiography. The processes occurring within the CCM during the first operating hours were visualized and first steps to unveil other degradation mechanisms will be shown.

2. Materials and Methods

2.1. Fabrication of the catalyst-coated membrane (CCM)

IrO_2 and Pt/C 9100 20% from Johnson&Matthey catalysts were added to a Nafion emulsion to reach 20 wt.% Nafion loading for the cathode catalyst and 25 wt.% for the anode in relation to the solids content. Afterwards, the suspension underwent ultrasonic treatment for homogenization. The final suspension was deposited on a PTFE foil substrate using the blade-coating method [30]. The electrodes were then dried in air for approx. 30–45 min and placed in a drying cabinet at 60 °C for 3 h. Conditioned and chain-stabilized Nafion 117 was used for the fabrication of the CCM. The membranes were treated beforehand with 20% H_2O_2 to remove any organic impurities and then rinsed in water at 80 °C. This was followed by a treatment in a 1

molL^{-1} H_2SO_4 bath to remove any metallic impurities. The conditioned membranes were then suspended in a flow-box drying chamber for at least two days. The dried Nafion 117 membranes were subsequently used for the fabrication of CCMs. A hydraulic press was heated to approx. 130 °C for this purpose. The electrodes were placed on top of each side of the membrane, hot pressed at 130 °C, and a pressure of 0.5–1 kN·cm^{-2} for 3–5 min. After delamination, the CCM was then ready for use. Iridium loading on the anode side was 2.2 mg_{Ir}·cm^{-2} and the platinum loading on the cathode side was 0.8 mg_{Pt}cm^{-2}. The electrode active area was 1 cm^2.

2.2. Cell assembly and synchrotron measurement conditions

Cell operation was visualized with the aid of synchrotron radiation, which was conducted at the BAMline on the electron storage ring BESSY II at Helmholtz-Zentrum Berlin. The intensity of synchrotron radiation transmitted through the cell was detected using a suitable detector system (50 µm CdWO4 scintillator, pco400 CCD camera). The spatial resolution of the detector system was 0.44 µm. The changes in the individual components of this cell structure were thus recorded temporally and spatially as 2D projections. The exposure time was set to 3 s to ensure a sufficiently high temporal resolution and good image statistics. Image processing followed the Beer–Lambert law in order to visualize the distribution of water and gas in the cell during operation.

2.3. Image processing

The Beer–Lambert law (equation 1) states that beam intensity is reduced by a factor dependent on the cell material and its attenuation coefficients as well as on the thickness of the material.

$$I = I_0 \cdot e^{-\sum \mu \cdot z} \qquad (1)$$

where I_0 is the original beam intensity, I the intensity of the transmitted beam, z the material thickness, and µ the absorption coefficient of the respective material. The water column thickness inside the PTL and flow-field channels can be determined when equation 1 is reformulated with z (equation 2).

$$z = \frac{-1}{\mu} \ln\left(\frac{I}{I_0}\right) \qquad (2)$$

In order to visualize bubble formation during cell operation, 20 successive radiographs were combined in one radiograph image, and corresponds to a period of 60 s. Due to the significantly faster dynamic processes occurring in the cell, only “stationary” structures such as the PTL structure and the catalyst layer are visible. In addition, each of the 20 radiographs was divided by the mean. This ensured that all fast changes, such as bubble growth and movement, were visible in the image. However, stationary information was no longer contained in the divided radiograph.

Gas bubbles appear brighter than the water-filled regions in the divided radiograph. This is due to the higher absorption of water. Table 1 presents a summary of the testing protocols and the results presented in Fig. 2 are discussed in the next section.

Table 1. Program sequence used in the operando electrolysis synchrotron experiments.

Program 0	
Time	1 h
Current	Off
Water Flow	Off
Program 1	
Time	4 h
Current	Variable (pol. Curve)
Water Flow	2 ml·min^{-1} (λ_{max}=250 @ 1.3 A·cm^{-2})
Program 2	
Time	2 h
Current	On and off every 10 min
Water Flow	2 ml·min^{-1} (λ_{max}=3000 @ 1.2 A·cm^{-2})
Program 3	
Time	1 h 10 min
Current	Variable (pol. Curve)
Water Flow	20 ml·min^{-1} (λ_{max}=3500 @ 1 A·cm^{-2})
Program 4	
Time	45 min
Current	On (0.6 A·cm^{-2}) and off every 10 min
Water Flow	20 ml·min^{-1} (λ_{max}=6000 @ 0.6 A·cm^{-2})
Program 5	
Time	1 h
Current	On (0.6 A·cm^{-2}) and off every 10 min
Water Flow	2 ml·min^{-1} (λ_{max}=600 @ 0.6 A·cm^{-2})
Program 6	
Time	1 h
Current	On (0.6 A·cm^{-2}) and off every 10 min
Water Flow	switching between 2 ml/min and 20 ml/min
Program 7	
Time	1 h 30 min
Current	On (0.6 A·cm^{-2}) and off every 10 min
Water Flow	20 ml/min

Results

Visualization of catalyst detachment

The cell was tested during a total time of 12 h and *in-operando* synchrotron radiography allowed the visualization of the changes in real-time. After 1 h, the first detachments of catalyst particles can be seen (Fig. 1). In order to quantify this effect, the image region with the anode catalyst was marked (red) and the change over-time determined for the mean transmitted beam intensity (Fig. 2). Iridium absorbs a good portion of radiation, and explains why the mean transmitted beam intensity is low at the beginning of the measurement: a grey-value of approx. 2000. Over-time, individual iridium particles detach from the catalyst layer and move along with the water–gas flow. The transmitted intensity increases due to the missing material in the red marked region. One can also observe that the iridium particle detachment starts on the electrode side facing the membrane. We expect that the electrode side facing the membrane is the most active region, since the electrode is in intimate contact to the electrolyte. In this region, intense gas-evolution is occurring, probably causing mechanical stress over the catalysts layer and eventually leading to its detachment. The side facing the PTL seems to be intact and resistant to material delamination.

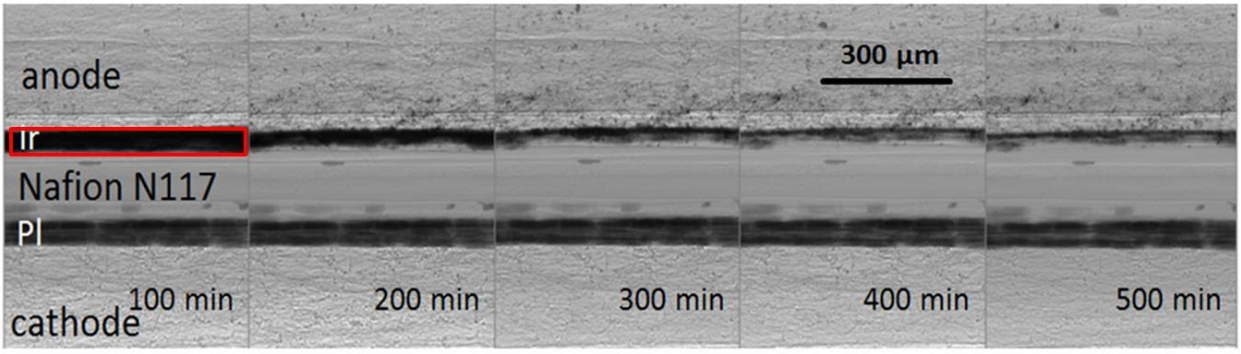

Figure 1 - Radiographic series of the development over time in the CCM, where iridium particles detachment is observed. Platinum particles in the cathode catalyst layer appear to be more stable, and no catalyst detachment is observed. The electrode side facing the membrane is subjected to extreme stress and faces the most severe delamination.

The transmitted intensity (I) does not just depend on the material in the beam path but also on the original beam intensity (I_0), see equation 1. To eliminate intensity fluctuations of the original beam intensity, the mean transmission intensity in the region of the membrane was determined. The middle region of the Nafion membrane remained unchanged throughout the entire measurement, so that fluctuations in beam intensity can be attributed to the intensity measurements in the membrane. In accordance with equations 3–6, we made the following assumptions: $I_1(t)$ is the transmitted beam intensity in the membrane region. $I_{1.0}$ is the transmitted beam intensity at the start of the measurement and c(t) is a time-dependent noise caused by fluctuations in the original beam intensity (equation 3). $I_2(t)$ is the transmitted beam intensity in the electrode region. The transmitted beam intensity in this instance depends on the original beam

intensity $I_{2.0}$ and the time-dependent noise c(t) (equation 4). Since in the case of the membrane, $I_{1.0}$ is the mean of $I_{1(t)}$, c(t) can be easily determined (equation 5). c(t) is constant in the entire image region. This is particularly true for the region showing the anode catalyst. On the basis of these considerations, fluctuations in the original beam intensity can be filtered out of the intensity of the beam transmitted in the anode region (equation 6).

$$I_1(t) = I_{1.0}\big(1 + c(t)\big) \tag{3}$$

$$I_2(t) = I_{2.0}\big(1 + c(t)\big) \tag{4}$$

$$c(t) = \frac{I_1(t) - I_{1.0}}{I_{1.0}} \tag{5}$$

$$I_{2.0}(t) = \frac{I_2(t)}{1 + c(t)} \tag{6}$$

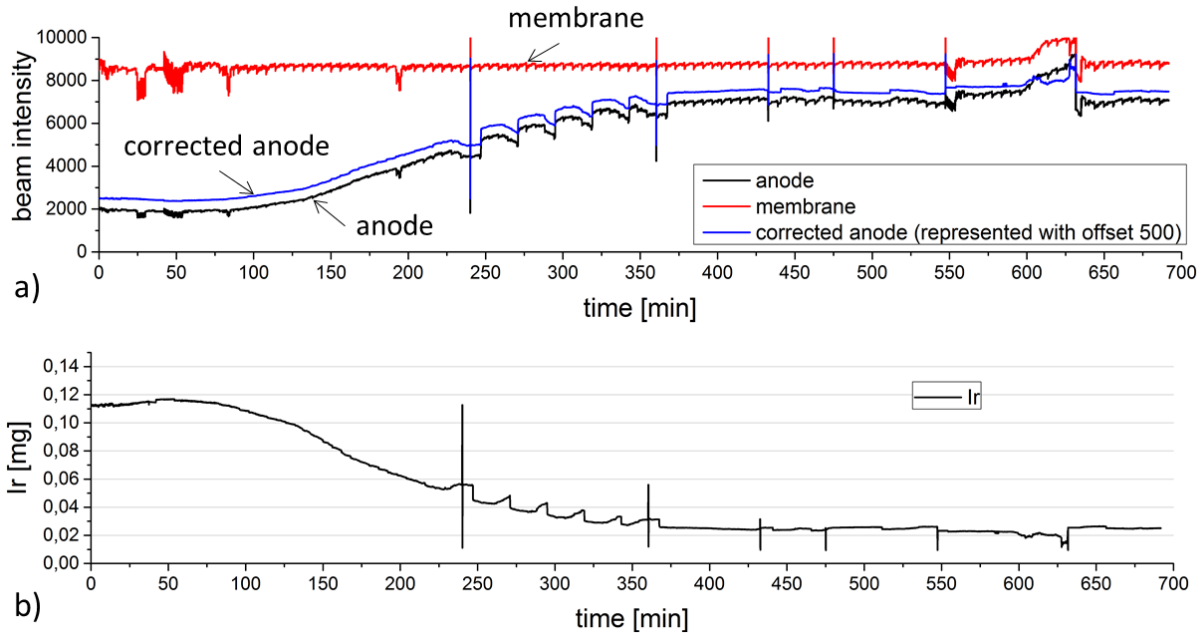

Figure 2a) Development over time of the mean transmitted beam intensity in the region of the anode catalyst and Nafion membrane; b) Development over time of the irradiated iridium mass in the anode catalyst. A 500 beam intensity offset was added to the blue curve for clarity.

In Fig. 2a, a beam intensity offset was used for better visual representation; otherwise, both curves would lie on top of each other making them difficult to distinguish. Large, vertical lines in the beam intensity curve were caused by the changes in the test program. However, catalyst detachment was independent of the test program. During the first two hours of cell operation, the catalyst layer remained unchanged. This was followed by a gradual reduction in catalyst layer thickness. After an operating time of approx. 6 h, no further changes were observed. The transmitted intensity has no physical unit. When this information is processed according to the Beer–Lambert law, the dimension of material layer thickness is given. Iridium is a heavy element

and plays a crucial role during energy absorption in the catalyst. At a beam energy of 25 keV, the absorption coefficient of iridium was 888 cm^{-1} and of carbon only 0.23 cm^{-1}. The iridium catalyst loading was 2.2 $mg \cdot cm^{-2}$. Now we can use the beam intensity values from Fig. 2a to also estimate the amount of iridium present in the catalyst layer, and a value of 0.11 mg iridium was obtained over the beam targeted area of 0.05 cm^2, that can be extrapolated to precisely 2.2 $mg \cdot cm^{-2}$. This estimate is therefore in very good agreement with the Ir loading measurement from the CCM fabrication. Prior to measurement, the amount of iridium was almost 0.12 mg (Fig. 2 b). After an operating time of 6 h, there was only 0.025 mg iridium left. After two hours of cell conditioning, more than 60 % of the iridium catalyst was lost through delamination processes most-likely caused by the initial mechanical stress inside the catalyst layer (gas evolution). This experiment clearly demonstrates how much catalyst material is still present on the CCM after the break-in procedure. A large proportion of the coated catalyst detached from the layer and was no longer involved in the electrochemical reaction. Here we see the important to optimize and improve electrode adhesion over the membrane [28, 31]. This would enable a threefold reduction in catalyst loading and also reduce costs for the same operating point.

Electrochemical characterization

In the second test program, the cell was operated dynamically. The current was switched on and off every 10 minutes and the voltage was recorded (Fig. 3). The curve progression reveals two different superimposed effects and shows changes in the gas–water content in the marked region. When the current was switched on, the gas produced displaced the water from the observed region. Gas considerably absorbs less radiation than water, which means the transmitted beam intensity increases. When the current was switched off, the voltage gradually declined. Gas was no longer produced and gas that had already been produced was displaced again by the water. Water absorbs more radiation than gas, which resulted in the transmitted beam intensity being reduced again. Consequently, this 10-min rhythm of increases and decreases in the transmitted beam intensity reflects the changes in the gas–water content in the catalyst layer.

Another important effect observed in the Fig. 3 is how the mean transmitted beam intensity increased despite regular operation without current. The increase is highlighted by a dashed auxiliary line in the graph and represents the influence of catalyst layer detachment. When the iridium particles diffused out of the observed region, less material was present in the beam path and the transmitted beam intensity increased.

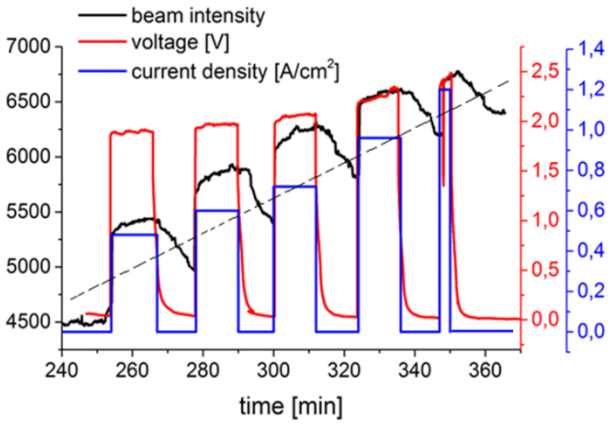

Figure 3 - Second measurement program with dynamic alteration of current. The transmission intensity shows the influence of water in the catalyst layer and degradation process.

Bubble formation

In accordance with the Beer–Lambert law, we were able to process the intensity images and visualize bubble formation and catalyst particle movement with a good temporal resolution of 2 s.

The following descriptions apply to the dynamic cell operation. The current and voltage curves are shown in Fig. 3.

Figure 4b) 0 Acm^{-2}, 0 V, t = 240 min

Without current flow, no bubble formation was observed. Movement was observed in the region of the anode catalyst and a number of particles moved along the catalyst layers. No movement was observed in the region of the cathode catalyst.

Figure 4c) 0.05 Acm^{-2}, 2 V, t = 250 min

When the current was switched on, bubble formation and movement of catalyst particles were observed. On the anode side, bubble formation was observed between the catalyst surface and the PTL, and many small bubbles were observed at the catalyst. The bubbles migrated through the PTL to the channel above and agglomerated to form larger bubbles. The distribution of bubbles in the PTL exhibited a certain gradient. Many small gas bubbles were visible directly at the catalyst. When migrating through the PTL, small bubbles agglomerated to form larger bubbles at the PTL region near the channel. With the increasing bubble size, the mean distance between the bubbles also increased. The distribution of water exhibited broad water pathways at the PTL–channel interface and increasingly branched out in the direction of the membrane. The same distribution of water was observed by Lee et al. [32]. Catalyst particles moved along the edge between the gas and water phases. We suspect that the movement of bubbles is the driving force behind catalyst particle movement and consequent detachment.

On the cathode side, bubble formation was observed between the Nafion membrane and the catalyst layer. The bubbles cannot, therefore, be discharged directly through the PTL into the channel (as occurs on the anode side), but first need to pass through the catalyst layer. Hydrogen

bubbles moved and grew, although they did not grow any larger than the gap between the catalyst coating and Nafion membrane allowed. Since the hydrogen bubbles did not have space to grow, they were forced to propagate through the porous catalyst coating. This resulted in a mechanical stress for the catalyst layer. Despite this stronger mechanical stress caused by the bubbles, only minimal changes were observed in the cathode catalyst layer. Although the same method was used to fabricate the anode and cathode catalyst layers, platinum (cathode side) appears to exhibit much better coating adhesion and stability than iridium (anode side).

Figure 4c) 0 Acm^{-2}, 1 V, t = 260 min

When the current was switched off, the voltage gradually declined. As the water was supplied to the anode side, it was possible to visualize the discharge of gas from the PTL. Oxygen bubbles remained in one spot, no longer moving but becoming smaller. The cathode side was not supplied with water. However, water diffused through the Nafion membrane [33-35] and since no current was available, no movement of bubbles could be visualized.

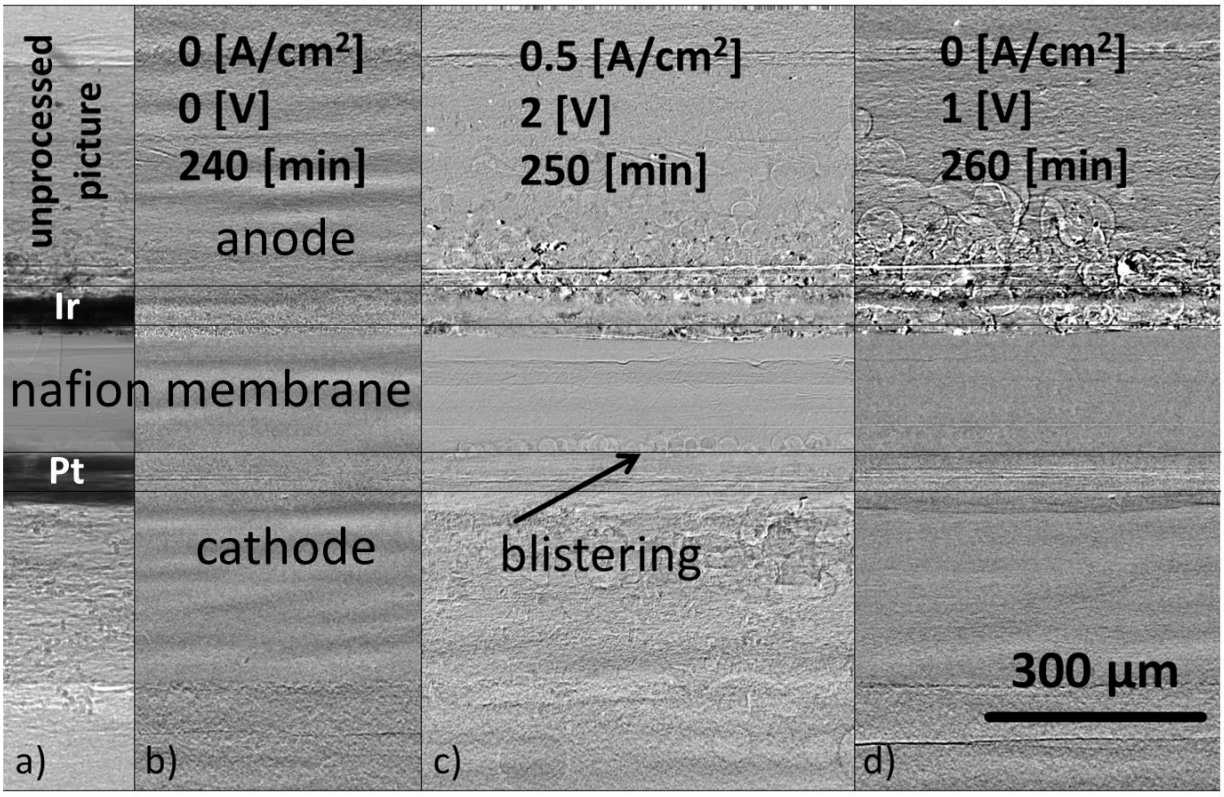

Figure 4 - Images showing the distribution of gas during the three operating points: a) an unprocessed image is shown as a reference; b) without current applied, bubble formation could not be observed; c) formation and distribution of gas bubbles at a current density of 0.5 Acm^{-2} ca be observed; d) diffusion of bubbles when the current was switched off; voltage gradually subsides. The times given refer directly to figure 3.

Particle characterization

Carbon papers used as PTLs have a porosity of approximately 75 % and the detached catalyst particles could freely move through the PTL pores. When looking at the trajectories of individual particles, two types of movement can be identified. The first typical movement is the tumbling of particles in one spot with minimal movement around one point. In other words, the particles move within one pore. The second movement is characterized by quick jumps, mostly in the form of movements in a straight line from one spot to another. The particles randomly move along the PTL thickness from one pore to the next, with the flow of water or a gas bubble.

The iridium particles absorb more intensity than carbon paper, which is why they appear darker in the image (Fig. 1). For this analysis, a mean was obtained from an image sequence of 6 images, which equates to a time interval of 6 s, this in order to reduce image noise. A threshold in the intensity was used to address the image noise of the particles. For the dark particles defined as catalyst particles, the area and number of individual particles was determined. It should be noted that several particles directly behind each other in the beam direction were evaluated and are considered as one particle. The threshold does not enable tracking of several particles or particles that partially or completely overlap. In general, more particles have detached than the graph shows (Fig. 5). To monitor the development of catalyst detachment over time, the images were analysed at intervals of 50 min.

The number of particles increased linearly from the second hour of operation until a total of 350 particles and a respective area of 0.014 cm^2 was achieved after 6 h operation. After this, only small fluctuations in the number of particles were observed. The mean area of particles also increased and it was between 30 μm^2 and 50 μm^2 after 6 h. The development of particle size distribution over time exhibited a significant peak in the range of 20 μm^2. The increase in particle area indicates the agglomeration of detached particles (Ostwald ripening) or that increasingly large particles detach over time. The iridium powder used for catalyst fabrication exhibited an identical particle size distribution with a peak at 20 μm^2. This indicates that when the catalyst detaches, individual original particles separate from the remaining layer.

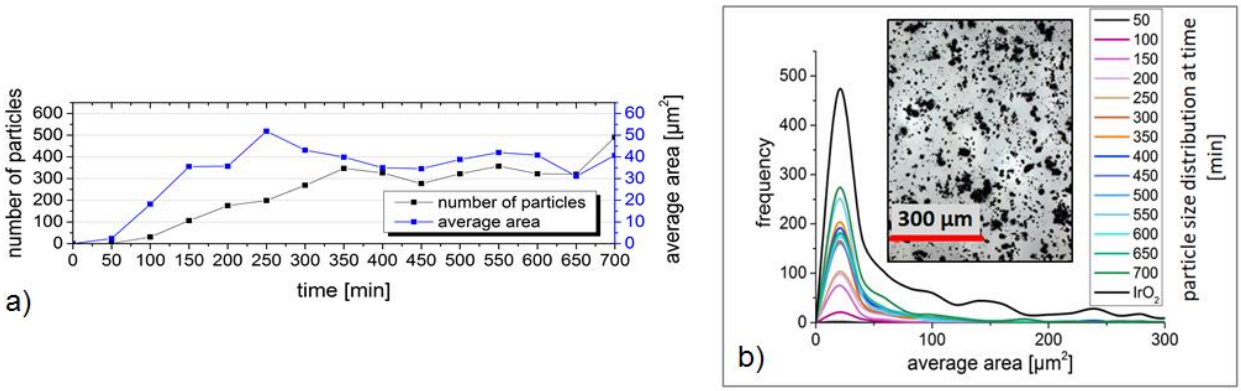

Figure 5 - a)Development over time of the number and size of the detached catalyst particles ; b)development over time of the particle size distribution of detached catalyst particles and catalyst powder, which was used to fabricate the catalyst layer.

We also investigated whether the thickness of the Nafion membrane decreased. The membrane thickness was measured with the aid of a profile line in the radiographs. The intensity values were averaged on the y-axis and the changes over time were monitored. The development and change in the Nafion membrane were monitored during the first current-voltage characteristic at intervals of 12 min. Fig. 6a shows the first and last image of the image series used for analysis. Severe degradation of the anode catalysts was observed. Fig. 6b shows the profile lines of the image series. The profile lines reveal catalyst erosion near the Nafion membrane and a deposition of catalyst particles in the PTL, in strong agreement to our observations from within Figure 1. A reduction in the thickness of the Nafion membrane could not be detected. Similar measurements on the same type of membrane were also conducted in operando on DMFCs [36]. A clear correlation was determined between increasing electrical loads and increasing thicknesses and the transmittance of the membrane.

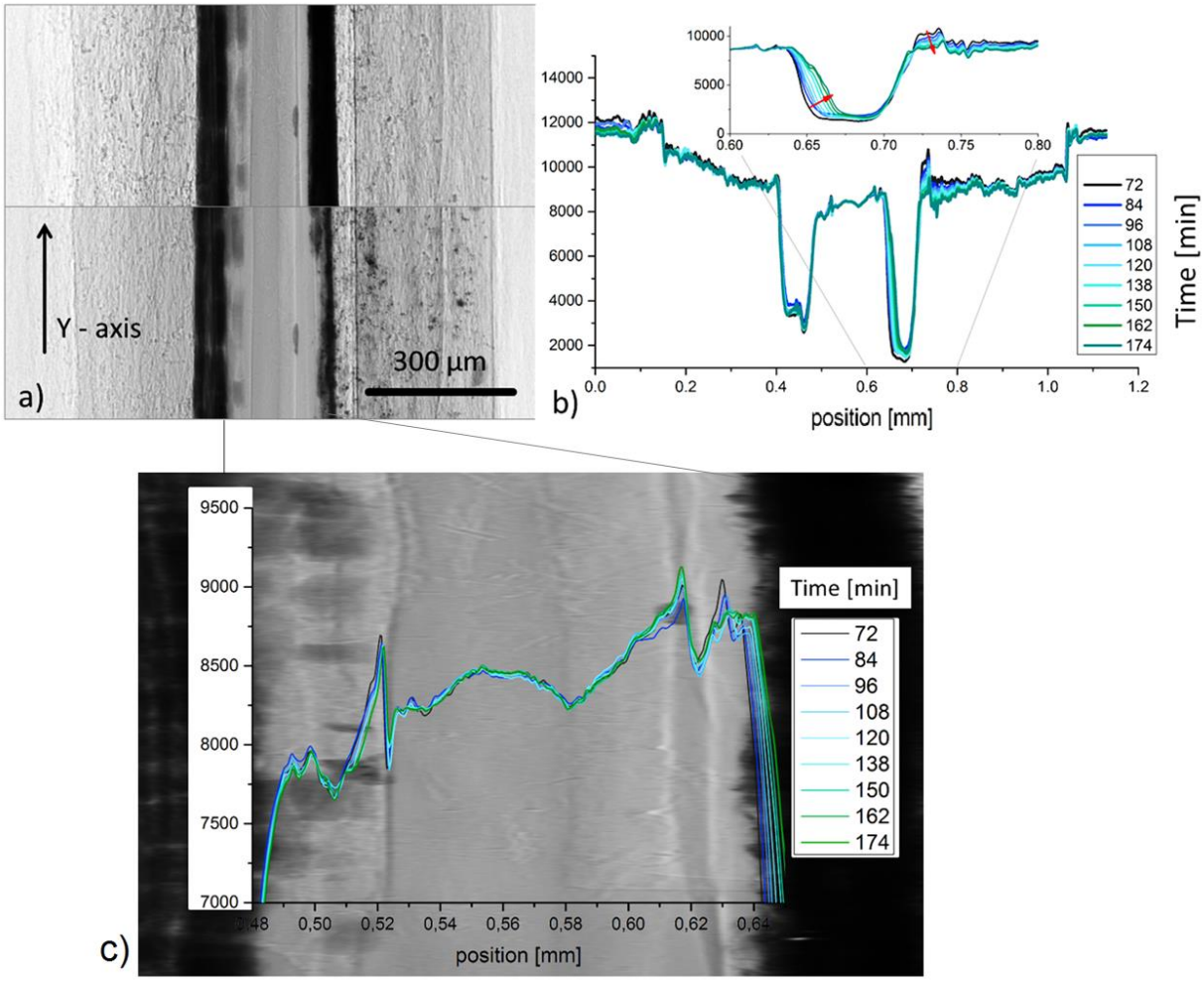

Figure 6 - a) Difference in CCM degradation at the start of the measurement and after 174 min; b) line profiles, averaged intensity on the y-axis, as a function of measurement time; c) changes in Nafion membrane.

Post-mortem analysis: TEM & FIB

After the measurement with synchrotron radiation, the entire cell in its original assembled state was cut in half. One half was disassembled and the CCM was analysed using focused ion-beam (FIB). The other half was embedded and the cross section polished for TEM and elemental analysis.

Using the FIB technique, a micro-cut was made perpendicular to the surface and the catalyst structure was analysed. Two FIB images are shown in Fig. 7. The particle structure and the pores can be well visualized. Remarkably, the platinum catalyst has a more homogeneous pore distribution. The particles themselves have an elongated shape and a length of approx. 200 nm. The anode catalyst with iridium has a more inhomogeneous pore distribution. Very fine-pored regions alternate with coarser structures with large pores. The number and surface area of the pores were calculated using an image processing program. The mean pore diameter was

1.801 µm for platinum and 1.746 µm for iridium. The large voids in the iridium electrode can be clearly related to the catalyst detachment observed in this work.

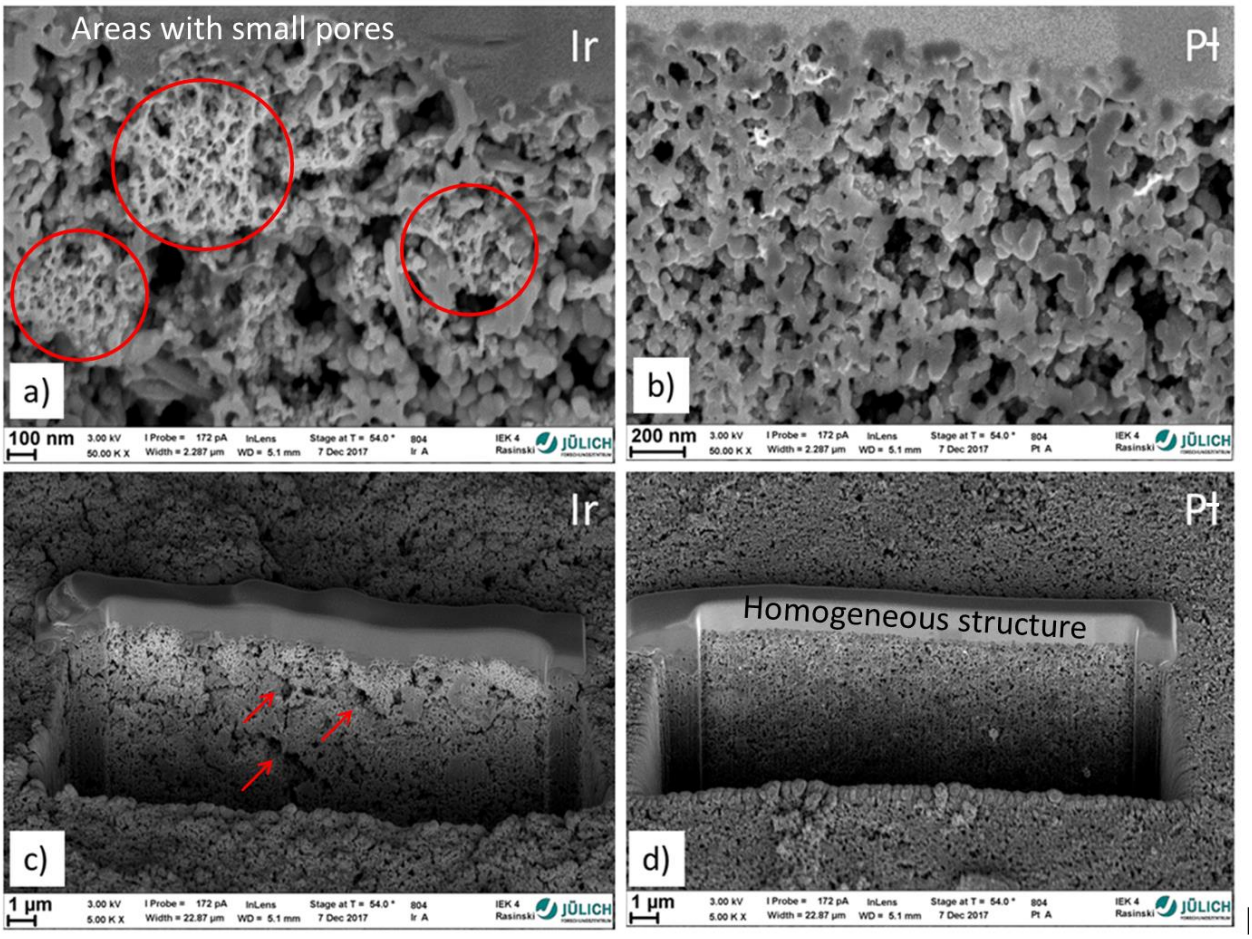

Figure 7 - FIB analysis of the catalyst coating: a) and c) Iridium layer as anode catalyst; b) and d) platinum layer as cathode catalyst.

For TEM investigation, one cell half was embedded and polished, and the distribution of elements was subsequently recorded, and the data is presented in the Fig. 8a. The middle part of the channel had no mechanical supports and therefore broke-off when cutting the cell. Nevertheless, the cell structure is easily recognizable. The Nafion membrane coated with the catalyst lies between the PTL and flow-field layers. Fig. 8b shows the distribution of chemical elements in the region and the particles are depicted in green. A number of rod-like platinum particles with a length of approx. 200 µm can be seen. Agglomerated platinum particles remain clustered together even after detachment of the layer. The iridium particles do not form large agglomerates and are therefore difficult to identify at a smaller resolution. In the image with higher resolution (Fig. 8b), both catalysts can be seen at both electrodes. No platinum or iridium catalysts were detected within the Nafion membrane.

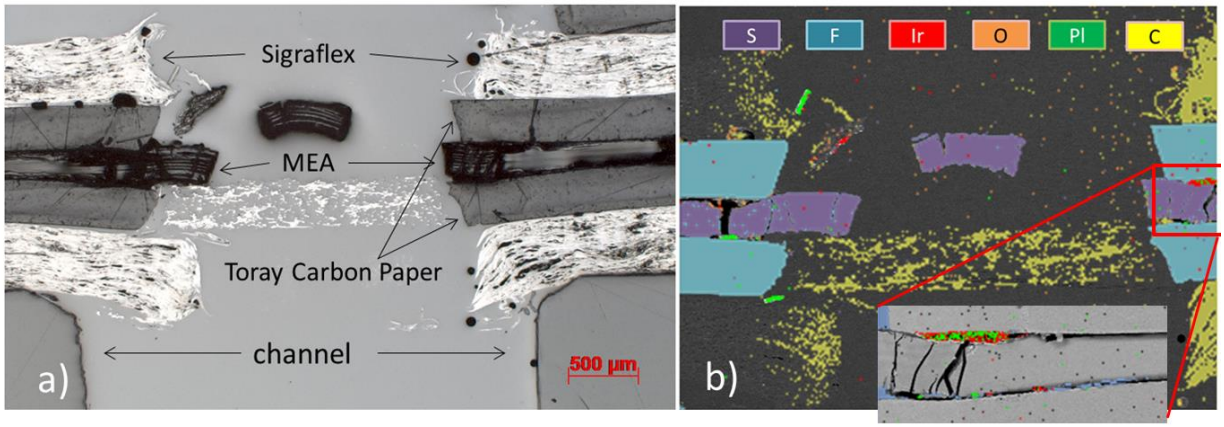

Figure 8a) Microscopic image of the cell cross section; b) SEM – elemental distribution analysis.

Discussion

In this work, the electrodes of a PEM electrolysis cell were real-time visualized during electrolysis operation. A noticeable degradation of the anode catalyst was detected. Here, we identified as the degradation mechanism of the iridium catalyst layer the detachment of individual catalyst particles caused by mechanical stress due to gas evolution. When iridium particles detach from the layer, the three-phase boundary region (i.e. water, Nafion, and catalyst) is no longer given. Therefore, the observed process of catalyst layer thinning can be observed and identified.

Both catalyst layers – anode and cathode – were fabricated using the method, but different additives were used, giving distinct adhesion properties over the membrane. Moreover, platinum particles are supported on carbon black, which gives additional adhesion strength when attaching over the membrane. As far as this work is concerned, degradation was only observed on the anode side and the cathode side remains almost unchanged. This contradicts the observations of Chandesris et al. [14], who observed degradation mainly on the cathode side. The difference in cell design, electrode fabrication, additives used, and testing protocols could be the reason for this disagreement. More work is therefore necessary to further unveil the discrepancies.

The visualization of bubble formation shows at which point the reaction occurs. When the water passed through the anode PTL and reached the catalyst layer, the electrochemical reaction took place, water was split and oxygen is formed. Released protons migrated through the Nafion membrane and, when they reached the catalyst layer on the cathode side, recombined with electrons to form hydrogen. The cell was positioned with the anode side facing upwards, which meant that the natural buoyancy of the bubbles was advantageous for mass transport. The visualization of bubble formation showed which part of the catalyst contributes to the electrochemical reaction. Since bubbles only formed on the catalyst surface, it was assumed that the upper catalyst layer was primarily involved in the reaction.

Thinning of Nafion membranes is expected to have a much longer time scale, and therefore could not be observed. The simulations conducted by Chandesris [14] showed a 50 % reduction in the Nafion membrane thickness only after 10,000 h operation.

Conclusion

Here we demonstrated real-time catalyst layer detachment in a PEM electrolysis cell, visualized by *in-operando* synchrotron radiography. The degradation process, which occurred during the cell break-in procedure, was remarkably observed during the first 8 h operation. The catalyst layer remained unchanged during the first hour of operation. After this, individual particles began to detach, and after 6 h, most of the particles were leached away from the electrode surface. The catalyst layer did not change noticeably after this. We also observed that the particles that diffused through the PTL had the same size distribution as the iridium powder used to fabricate the catalyst layer.

The movement of gas bubbles in the PTL could also be visualized. Hydrogen formed on the cathode side between the Nafion membrane and the catalyst layer. This demonstrates that the oxidation reaction occurs very quickly and that only the nearby catalyst layer participates in the reaction. On the anode side, oxygen bubbles formed at the boundary between the catalyst layer and the PTL. We concluded that the oxygen bubbles represent the driving force for the detachment of the catalyst particles.

The catalyst structure was also analyzed using FIB, revealing that the platinum catalyst had a more homogeneous pore structure and pore shape than the iridium catalyst. The mean pore diameter was approx. 1.8 µm for Pt and approx. 1.75 µm for Ir. The spatial resolution of chemical elements showed that both platinum and iridium were found on both electrodes. Mutual catalyst migration took place. No platinum or iridium band was detected inside the membrane.

Acknowledgements

The authors would like to thank HZB for the beam time and numerous scientific discussions. We would also like to thank Elena Borgardt, Andreas Everwand, Michael A. Hoeh, Richard Wegner, Christian Bordin, Roger Keller, Norbert Commerscheidt, and Juri Romazanov (all at Forschungszentrum Jülich). Furthermore, financial support within the NestPEL project provided by the German Federal Ministry for Economic Affairs and Energy (BMWi, Förderkennzeichen 03ET6044A) is highly appreciated.

Literature

[1] X. Huang, Q. Meng, H. Chen, X. Du, L. Chen, Renewable energy conversion, storage, and efficient utilization, Science, 360 (2018) 47-51.
[2] G. Wagner, T. Kåberger, S. Olai, M. Oppenheimer, K. Rittenhouse, T. Sterner, Energy policy: Push renewables to spur carbon pricing, Nature News, 525 (2015) 27.
[3] D. Stolten, V. Scherer, Transition to renewable energy systems, John Wiley & Sons, 2013.
[4] M. Carmo, D.L. Fritz, J. Mergel, D. Stolten, A comprehensive review on PEM water electrolysis, International Journal of Hydrogen Energy, 38 (2013) 4901-4934.

[5] M. Carmo, D. Stolten, Energy Storage Using Hydrogen Produced From Excess Renewable Electricity: Power to Hydrogen, in: Science and Engineering of Hydrogen-Based Energy Technologies, Elsevier, 2019, pp. 165-199.
[6] K.A. Friedrich, P. Lettenmeier, S. Stiber, A.S. Ansar, L. Wang, A.S. Gago, Cost-Effective PEM Electrolysis: The Quest to Achieve Superior Efficiencies with Reduced Investment, in: Meeting Abstracts, The Electrochemical Society, 2018, pp. 15-15.
[7] K.E. Ayers, J.N. Renner, N. Danilovic, J.X. Wang, Y. Zhang, R. Maric, H. Yu, Pathways to ultra-low platinum group metal catalyst loading in proton exchange membrane electrolyzers, Catalysis Today, 262 (2016) 121-132.
[8] S.M. Saba, M. Müller, M. Robinius, D. Stolten, The investment costs of electrolysis–a comparison of cost studies from the past 30 years, International Journal of Hydrogen Energy, 43 (2018) 1209-1223.
[9] C. Rakousky, U. Reimer, K. Wippermann, M. Carmo, W. Lueke, D. Stolten, An analysis of degradation phenomena in polymer electrolyte membrane water electrolysis, Journal of Power Sources, 326 (2016) 120-128.
[10] P. Millet, N. Mbemba, S. Grigoriev, V. Fateev, A. Aukauloo, C. Etiévant, Electrochemical performances of PEM water electrolysis cells and perspectives, International Journal of Hydrogen Energy, 36 (2011) 4134-4142.
[11] K.E. Ayers, E.B. Anderson, C. Capuano, B. Carter, L. Dalton, G. Hanlon, J. Manco, M. Niedzwiecki, Research advances towards low cost, high efficiency PEM electrolysis, ECS Transactions, 33 (2010) 3-15.
[12] N. Yousfi-Steiner, P. Moçotéguy, D. Candusso, D. Hissel, A review on polymer electrolyte membrane fuel cell catalyst degradation and starvation issues: Causes, consequences and diagnostic for mitigation, Journal of Power Sources, 194 (2009) 130-145.
[13] S. Zhang, X.-Z. Yuan, J.N.C. Hin, H. Wang, K.A. Friedrich, M. Schulze, A review of platinum-based catalyst layer degradation in proton exchange membrane fuel cells, Journal of Power Sources, 194 (2009) 588-600.
[14] R. Borup, J. Meyers, B. Pivovar, Y.S. Kim, R. Mukundan, N. Garland, D. Myers, M. Wilson, F. Garzon, D. Wood, Scientific aspects of polymer electrolyte fuel cell durability and degradation, Chemical reviews, 107 (2007) 3904-3951.
[15] A. Laconti, H. Liu, C. Mittelsteadt, R. McDonald, Polymer electrolyte membrane degradation mechanisms in fuel cells-findings over the past 30 years and comparison with electrolyzers, ECS Transactions, 1 (2006) 199-219.
[16] S. Grigoriev, K. Dzhus, D. Bessarabov, P. Millet, Failure of PEM water electrolysis cells: Case study involving anode dissolution and membrane thinning, International Journal of Hydrogen Energy, 39 (2014) 20440-20446.
[17] J. Péron, Y. Nedellec, D.J. Jones, J. Rozière, The effect of dissolution, migration and precipitation of platinum in Nafion®-based membrane electrode assemblies during fuel cell operation at high potential, Journal of Power Sources, 185 (2008) 1209-1217.
[18] L. Kim, C.G. Chung, Y.W. Sung, J.S. Chung, Dissolution and migration of platinum after long-term operation of a polymer electrolyte fuel cell under various conditions, Journal of Power Sources, 183 (2008) 524-532.
[19] M. Debe, S. Hendricks, G. Vernstrom, M. Meyers, M. Brostrom, M. Stephens, Q. Chan, J. Willey, M. Hamden, C.K. Mittelsteadt, Initial performance and durability of ultra-low loaded NSTF electrodes for PEM electrolyzers, Journal of the Electrochemical Society, 159 (2012) K165-K176.
[20] C. Rakousky, U. Reimer, K. Wippermann, S. Kuhri, M. Carmo, W. Lueke, D. Stolten, Polymer electrolyte membrane water electrolysis: Restraining degradation in the presence of fluctuating power, Journal of Power Sources, 342 (2017) 38-47.
[21] S. Cherevko, A.A. Topalov, A.R. Zeradjanin, G.P. Keeley, K.J. Mayrhofer, Temperature-dependent dissolution of polycrystalline platinum in sulfuric acid electrolyte, Electrocatalysis, 5 (2014) 235-240.

[22] E. Kötz, S. Stucki, Ruthenium dioxide as a hydrogen-evolving cathode, Journal of applied electrochemistry, 17 (1987) 1190-1197.
[23] K.J. Mayrhofer, S.J. Ashton, J.C. Meier, G.K. Wiberg, M. Hanzlik, M. Arenz, Non-destructive transmission electron microscopy study of catalyst degradation under electrochemical treatment, Journal of Power Sources, 185 (2008) 734-739.
[24] K.J. Mayrhofer, J.C. Meier, S.J. Ashton, G.K. Wiberg, F. Kraus, M. Hanzlik, M. Arenz, Fuel cell catalyst degradation on the nanoscale, Electrochemistry Communications, 10 (2008) 1144-1147.
[25] P. Paciok, M. Schalenbach, M. Carmo, D. Stolten, On the mobility of carbon-supported platinum nanoparticles towards unveiling cathode degradation in water electrolysis, Journal of Power Sources, 365 (2017) 53-60.
[26] M. Shviro, M. Gocyla, S. Polani, M. Heggen, D. Zitoun, R.E. Dunin-Borkowski, Morphological, Structural, and Compositional Evolution of Pt–Ni Octahedral Electrocatalysts with Pt-Rich Edges and Ni-Rich Core: Toward the Rational Design of Electrocatalysts for the Oxygen Reduction Reaction, Particle & Particle Systems Characterization, (2019) 1800442.
[27] A. Burdzik, M. Stähler, I. Friedrich, M. Carmo, D. Stolten, Homogeneity analysis of square meter-sized electrodes for PEM electrolysis and PEM fuel cells, Journal of Coatings Technology and Research, 15 (2018) 1423-1432.
[28] F. Scheepers, A. Stähler, M. Stähler, M. Carmo, W. Lehnert, D. Stolten, Layer Formation from Polymer Carbon-Black Dispersions, Coatings, 8 (2018) 450.
[29] C. Liu, M. Carmo, G. Bender, A. Everwand, T. Lickert, J.L. Young, T. Smolinka, D. Stolten, W. Lehnert, Performance enhancement of PEM electrolyzers through iridium-coated titanium porous transport layers, Electrochemistry Communications, 97 (2018) 96-99.
[30] M. Carmo, G.P. Keeley, D. Holtz, T. Grube, M. Robinius, M. Müller, D. Stolten, PEM water electrolysis: Innovative approaches towards catalyst separation, recovery and recycling, International Journal of Hydrogen Energy, 44 (2019) 3450-3455.
[31] F. Scheepers, A. Staehler, M. Staehler, M. Carmo, W. Lehnert, D. Stolten, A new setup for the quantitative analysis of drying by the use of gas-phase FTIR-spectroscopy, Review of Scientific Instruments, 89 (2018) 083102.
[32] J. Lee, J. Hinebaugh, A. Bazylak, Synchrotron X-ray radiographic investigations of liquid water transport behavior in a PEMFC with MPL-coated GDLs, Journal of power sources, 227 (2013) 123-130.
[33] M. Watanabe, Y. Satoh, C. Shimura, Management of the water content in polymer electrolyte membranes with porous fiber wicks, Journal of The Electrochemical Society, 140 (1993) 3190-3193.
[34] X. Ren, S. Gottesfeld, Electro-osmotic drag of water in poly (perfluorosulfonic acid) membranes, Journal of the Electrochemical Society, 148 (2001) A87-A93.
[35] M. Schalenbach, M. Carmo, D.L. Fritz, J. Mergel, D. Stolten, Pressurized PEM water electrolysis: Efficiency and gas crossover, International Journal of Hydrogen Energy, 38 (2013) 14921-14933.
[36] T. Arlt, A. Schroeder, K. Heyne, H. Riesemeier, K. Wippermann, W. Lehnert, I. Manke, In-operando investigation of the humidity condition and the swelling of a Nafion-based membrane in a DMFC with synchrotron X-ray imaging, Journal of Power Sources, 297 (2015) 83-89.